Journal of Energy Storage 90 (2024) 111801

Contents lists available at ScienceDirect

Journal of Energy Storage

journal homepage: www.elsevier.com/locate/est

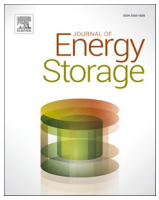

Research papers

Limit capacitance of the constant phase element

Enrique H. Balaguera [a,*], Anis Allagui [b,c]

[a] Escuela Superior de Ciencias Experimentales y Tecnología, Universidad Rey Juan Carlos, C/ Tulipán, s/n, 28933 Móstoles, Madrid, Spain
[b] Department of Sustainable and Renewable Energy Engineering, University of Sharjah, PO Box 27272, Sharjah, United Arab Emirates
[c] Department of Electrical and Computer Engineering, Florida International University, Miami, FL33174, United States of America

ARTICLE INFO

Keywords:
CPE
Dispersive capacitance
Time-constant distribution
Impedance Spectroscopy
Transient analysis
Fractional calculus

ABSTRACT

The constant-phase element (CPE) is a universal electrical model widely used to describe the intricate nature of a multitude of materials and processes under real-world conditions. The physical interpretation of the corresponding anomalous phenomenology is a challenging task, which traditionally relies on calculating an effective capacitance in the sense of a classical charge accumulation. However, a picture of this electrical element is not yet complete for cases of practical interest, and many questions remain open in relation to the intrinsic characteristics that makes it "unphysical" at long time scales. In this work, we derive mathematical formulas for estimating the limit capacitance of the CPE associated with surface and normal time-constant distributions. For this purpose, we obtain the transient responses, in term of multi-exponential relaxation patterns, attributable to the charge processes of micro-capacitances that constitute the "macroscopic CPE" with a dynamical behavior described in terms of the Mittag-Leffler function. As both transient dynamics can be considered negligible in practice from a certain time instant, we subsequently find the limit capacitance from a direct comparison of both steady-state times in the style of CPE reference works. Simulations are used to show that the obtained limit capacitance yields reasonable values for cases of multidisciplinary interest. Our study contributes to the advanced understanding of the pervasive presence of the CPE in natural and engineering contexts, shedding light on the problem of infinite charge and energy in complex systems.

1. Introduction

In elementary electrical engineering courses, everything looked simple: A capacitor was an electrical component that consists of two parallel-plate conductors separated by an insulating or dielectric material [1]. Now we know that capacitive effects can be also found in complex relaxation dynamics from physics [2,3] to life sciences [4,5]. The existence of microdomain-type structural and/or energetic heterogeneities that influence the ionic motion and charge transfer in physical systems causes an anomalous behavior of energy storage that deviates from a classical ideal capacitive behavior. This is the case, for instance, in electrochemical double-layers [6,7], space-charge accumulation zones [8,9] or cell membranes [10–12]. Perhaps more remarkable is the fact that even nanoscale structures behave anomalously at relevant timescales [13], challenging our view of charge accumulation processes. And now that complex systems and the investigation of their dynamical properties have been established on the modern physics agenda, important methodological efforts are needed to understand and mathematically describe the nature of this universal dielectric response.

Recall that for the classical capacitor, based on phenomena associated with electric fields, the current $i_C(t)$ is proportional to the rate at which the voltage $v_C(t)$ across its terminals varies with time; that is, $i_C(t) = C\,\mathrm{d}v_C(t)/\mathrm{d}t$. Thus, the associated impedance takes the basic form $Z_C(\omega) = 1/j\omega C$. In practice however many physical systems exhibit a non-ideal capacitive behavior manifested through frequency dispersion patterns or slow and persistent long-tailed transient phenomena [14]. Almost one century ago Cole introduced the concept of the *constant-phase element* (CPE) as a phenomenological function to fit the non-Debye relaxation forms in frequency-domain [15] connecting it, years later, to the Curie-von-Schweidler law [16]. During all these years, the associated electrical component has been ubiquitously employed at all scales in a wide variety of scientific fields, including electrochemistry, electronics, and biology. Therefore, millions of articles have been published on the experimental effects of CPE to explain the "imperfect capacitive phenomena" of multiple processes and materials. Deviations from such ideal behavior display an asymptotic power-law dependence in the frequency and time space [17], yielding the famous impedance of the

* Corresponding author.
E-mail address: enrique.hernandez@urjc.es (E. H. Balaguera).

https://doi.org/10.1016/j.est.2024.111801
Received 6 November 2023; Received in revised form 13 March 2024; Accepted 19 April 2024
Available online 11 May 2024

CPE:

$$Z_{\mathrm{CPE}}(\omega) = \frac{1}{Q(j\omega)^{\alpha}} \tag{1}$$

and the mathematically equivalent current-voltage relationship represented by the following fractional-order differential equation [18]:

$$i_{\mathrm{CPE}}(t) = Q\frac{\mathrm{d}^{\alpha}v_{\mathrm{CPE}}(t)}{\mathrm{d}t^{\alpha}} \tag{2}$$

Here, Q and α are the CPE parameters that exhibit an intrinsic coupling [19]. Specifically, Q represents a pseudo-capacitance in units of $\mathrm{F}/(\mathrm{cm}^2\mathrm{s}^{1-\alpha})$ and α is a dispersion coefficient ($0 < \alpha < 1$) related to the level of inhomogeneities in the geometric and/or energetic landscape of the material under study. It is clear that the parameter Q cannot represent the capacitance when $\alpha < 1$. Only a CPE with an exponent $\alpha = 1$ can model a capacitor in the sense of a corresponding energy conservation. For the case of the CPE, however, an energy dissipation emerges combined with the classical charge accumulation that happens naturally in the conventional version. Therefore, this "leaking capacitor" behaves as a mixed resistive-capacitive element,

$$Z_{\mathrm{CPE}}(\omega) = \frac{cos\left(\alpha\pi/2\right)}{Q\omega^{\alpha}} - \mathrm{j}\frac{sin\left(\alpha\pi/2\right)}{Q\omega^{\alpha}} \tag{3}$$

exhibiting both real and imaginary parts ($Z_{\mathrm{CPE,r}}(\omega)$ and $Z_{\mathrm{CPE,j}}(\omega)$, respectively) in the impedance and a constant, frequency-independent phase angle, $-\alpha\pi/2$ [20].

The framework on which basic capacitive behavior is based robustly enables to trace a physical interpretation of real-world processes, but the CPE challenges most of established paradigms [21,22]. The first introductory idea for devising adequately parallelisms with the classical theory was the estimation of an effective capacitance [23] arises by simply comparing the impedance of the capacitor with only the imaginary part of the impedance of the CPE:

$$C_{\mathrm{CPE}}(\omega) = \frac{1}{j\omega Z_{\mathrm{CPE,j}}(\omega)} = \frac{Q\omega^{\alpha-1}}{sin\left(\alpha\pi/2\right)} \tag{4}$$

resulting in a frequency-varying value with scale-invariant memory [24] and an infinite mode that, however, does not coincide with the result obtained from the real part of the complex capacitance, $C^{*}_{\mathrm{CPE}}(\omega) = {}^{1}/_{j\omega Z_{\mathrm{CPE}}(\omega)} = C^{*}_{\mathrm{CPE,r}}(\omega) + \mathrm{j}C^{*}_{\mathrm{CPE,j}}(\omega)$ [25,26]:

$$C_{\mathrm{CPE}}(\omega) = C^{*}_{\mathrm{CPE,r}}(\omega) = Q\omega^{\alpha-1}sin\left(\alpha\pi/2\right) \tag{5}$$

In fact, the CPE can be modeled by an infinite RC network [27] in which the resistors and capacitors in successive branches are related by a scaling factor in the sense of a fractal network [28,29]. Nevertheless, fractals in the natural and applied sciences are simply mathematical models, where the magnification is limited by the microscopic structure. Thus, a realistic and truncated version of the CPE is indeed needed to obtain a consistent view of the physical processes under study.

The recurrent observation of dispersive capacitance has driven considerable theoretical and experimental efforts for estimating an effective capacitance from the understanding of its origin and underlying mechanisms [30,31]. However, consensus statements for an adequate physical interpretation and mathematical treatment remain obscure and perplexing even after decades of research and debate. Specifically, consider the modified Randles circuit of Fig. 1(a), consisting of a resistor R_s in series with the parallel combination of a CPE and another resistor R_p, that represents the most typical equivalent circuit in which a CPE behavior emerges in nature. The exploration of an effective capacitance for the CPE has provided a palette of advanced microscale models characterized by different time-constant distributions, surface or normal (shown in Figs. 1(b) and 1(c), respectively) depending on the type of local variation on the anomalous capacitive properties, where the most relevant mathematical formulas are those of Brug et al. [32] and Hsu and Mansfeld [33]. From the literature, it is evident that the

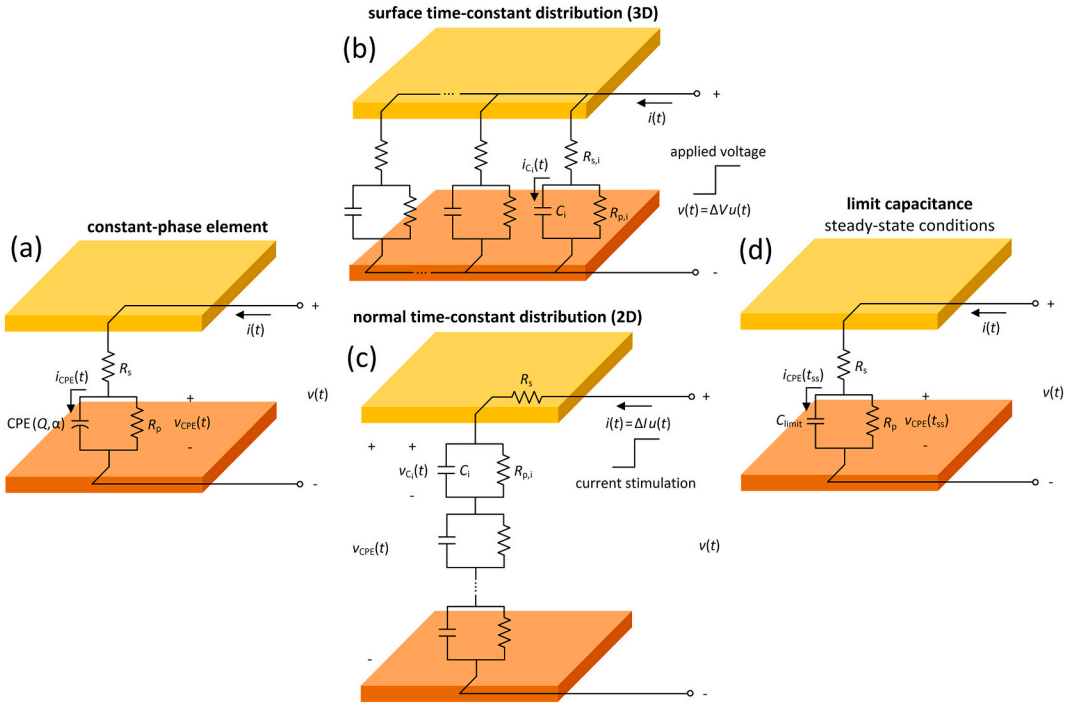

Fig. 1. (a) General Randles circuit with the introduction of a CPE as a classical result of macroscale electrical observations, and the equivalent models at microscale level corresponding to (b) surface and (c) normal distribution of time constants. Note that, in theory, the time-constant distributions of (b) and (c) are voltage- and current-controlled functions. (d) Electrical representation of the equivalent circuit shown in (a) under steady-state conditions when the CPE can be considered ideally capacitive.

origin of the CPE is a distribution of time constants, resulting in two- (2D) or three-dimensional (3D) capacitance dispersions from effects associated to current/voltage distribution along a surface or processes related to structural heterogeneity (geometric irregularities such as roughness, porosity, and varying composition) normal to the surface of the material under study, respectively [34]. By treating these surface or normal distributions of time constants illustrated in electrical terms by Figs. 1(b) and 1(c), respectively, the most important scheme developed in these elegant models of [32,33] assumes that the CPE does not exhibit a capacitive behavior per se but instead be coupled to the resistive properties of the system as:

$$C_{\text{eff}} = Q^{1/\alpha} R_{\text{Th}}^{(1-\alpha)/\alpha} = \begin{cases} Q^{1/\alpha}\left(\dfrac{R_s R_p}{R_s + R_p}\right)^{(1-\alpha)/\alpha} & \text{surface distribution} \\ Q^{1/\alpha} R_p^{(1-\alpha)/\alpha} & \text{normal distribution} \end{cases} \tag{6}$$

requiring the determination of the Thévenin resistance R_{Th} corresponding to the impedance (2D) or admittance (3D) response –$R_{\text{Th}} = R_p$ or $R_{\text{Th}} = R_s R_p / R_s + R_p$, respectively– of the phenomenon under study [35]. Remember that theoretically in impedance, the current is the input and the voltage is the output and vice versa for admittance, which has a significant impact on the calculation of the resistance "seen" from the CPE terminals (R_{Th}) when the input is deactivated. It is also important to note that, for the case of a 2D time-constant distribution, $C_{\text{eff}} \sim Q^{1/\alpha} R_s^{(1-\alpha)/\alpha}$ if $R_s \ll R_p$.

From this last scenario focused on an equivalent circuit consisting of a series combination of R_s and a CPE (with $R_p \to \infty$), it has been developed, during the last few years, a mathematical formulation to find an equivalent capacitance through time transient analysis. In this context, the presence of inherent memory in the CPE, as a resulting property of the fractional-order derivative of Eq. (2) [36,37], forms a complex problem due to the reciprocity properties of current and voltage for charging an electrical circuit with a CPE [38]. In fact, it results that the effective capacitance estimated via transient dynamics is dependent of the type and nature of the excitation. Note that this observation is in line with Eq. (6), which theoretically considers sinusoidal excitations of voltage (admittance) or current (impedance) as stimuli to analyze surface or normal time-constant distributions, respectively [35]. By considering a voltage or current input in form of $v(t) = \Delta v\left(t/\Delta t\right)^n$ or $i(t) = \Delta i\left(t/\Delta t\right)^n$, respectively, and subsequently comparing the electrical charge at long time scales or the current transient dynamics with the ideal RC circuit, Allagui et al. derived particular relations [38,39] that, expressed in a general way, yield:

$$C_{\text{CPE}}(t) = \begin{cases} \dfrac{\Gamma(n)}{(n-\alpha)\Gamma(n-\alpha)} Q t^{1-\alpha} & \text{applied voltage} \\ \dfrac{(\alpha+n)\Gamma(\alpha+n)}{(n+1)\Gamma(n+1)} Q t^{1-\alpha} & \text{current stimulation} \end{cases} \tag{7}$$

with a ratio of effective capacitances, $\Delta c = \Gamma(n)\Gamma(n+2)/(\alpha+n)\Gamma(n-\alpha+1)\Gamma(\alpha+n)$, that is independent of the time and the pseudo-capacitance Q, and is only function of α. Nevertheless, Eqs. (4), (5), and (7) show that the estimated effective capacitances of the CPE increase, without limit, proportionally to $\omega^{\alpha-1}$ (as frequency decreases) and to $t^{1-\alpha}$, respectively. That is, capacitance of the CPE never reaches a final value, which means the materials under study charge goes to infinity! [40,41] As previously commented on, it cannot physically exist and thus, this means that there is a specific instant beyond the measured range in which the CPE must become ideally capacitive.

All of these important physics-based models, developed during almost one century, that determine an ideal capacitance from the CPE parameters require further advancements to guide end-users for the optimal interpretation of anomalous dynamical responses with dispersive traces for each specific application. Mathematical approaches developed for the ubiquitous CPE involve continuous additive contributions in form of infinite capacitances, i.e., the material is continuously charged. From a physical point of view, such process is not realizable and therefore, a distribution of capacitance cannot exist in the whole frequency or time domain. The CPE must become purely capacitive at long time scales to be physically possible. Thus, it is important to decipher the limit capacitance encoded in the transient and steady-state responses and thus to better understand the charging process of this dispersive element. This will also allow to entirely emulate the anomalous behavior of the CPE, via electrical and electronic circuits [42]. We here augment the understanding of the CPE for decoding experimental data of time transients or impedance with anomalous dynamics (visually detectable as long-time tails or vertically depressed arcs in the complex plane representation and quantifiable as power-law patterns), in order to include an estimate of the real capacitance from numerical approximations. Our model provides unique and physically coherent insights into the quantification of a limit capacitance associated with the CPE that commonly models real-world processes, such as interfacial regions, space charge zones or cell membranes in electrochemistry, electronics or neurosciences, respectively, where, by nature, the self-similar spatial distributions of the material properties are limited.

2. Mathematical approach

Let us consider the most basic case collected in the old textbooks dealing with network analysis and control engineering [43,44] consisting of the analysis of the step response. Having studied the RC circuit, which is the most basic electrical model, we turn our attention that a classical capacitor does not respond immediately to stimuli; rather, the current and voltage, respectively, decays and rises exponentially toward a final term. In the models under study here, circuit theory shows that the external current response to a step voltage $v(t) = \Delta V u(t)$ and that corresponding to the capacitive effects in the "microscale equivalent circuit" with additive components from each part of the surface shown in Fig. 1(b) can be expressed as:

$$i(t) = \sum_i \frac{\Delta V}{R_{s,i} + R_{p,i}} \left(1 + \frac{R_{p,i}}{R_{s,i}} e^{-\frac{R_{s,i}+R_{p,i}}{R_{s,i}R_{p,i}C_i}t}\right) \tag{8}$$

$$i_{C,i}(t) = \sum_i \frac{\Delta V}{R_{s,i}} e^{-\frac{R_{s,i}+R_{p,i}}{R_{s,i}R_{p,i}C_i}t} \tag{9}$$

On the other hand, the transient voltages in response to a step current $i(t) = \Delta I u(t)$ in the electrical circuit of Fig. 1(c) with consecutive contributions through a layer are similarly:

$$v(t) = \Delta I R_s + \sum_i \Delta I R_{p,i}\left(1 - e^{-\frac{t}{R_{p,i}C_i}}\right) \tag{10}$$

$$v_{C,i}(t) = \sum_i \Delta I R_{p,i}\left(1 - e^{-\frac{t}{R_{p,i}C_i}}\right) \tag{11}$$

where $R_{s,i}$ is the local series resistance and $R_{p,i}$ and C_i represent the microscale properties at the surface (Eqs. (8) and (9)) or along the layer (Eqs. (10) and (11)) [45]. Note that R_s in the electrical model shown in Fig. 1(c) (Voigt configuration) represents a macroscale behavior because the appearance of a CPE behavior does not require its contribution [35,46]. The general measurement model, developed from impedance analysis, is based on the admittance and impedance expressions $Y(\omega) = \sum_i \left[R_{s,i} + \left(R_{p,i}/1 + j\omega R_{p,i}C_i\right)\right]^{-1}$ and $Z(\omega) = R_s + \sum_i R_{p,i}/1 + j\omega R_{p,i}C_i$ for surface and normal time-constant distributions, respectively [32,33].

The reason is that $Y(\omega)$ and $Z(\omega)$ include additive contributions from each part of the material surface (parallel connection of simplified Randles circuits) and from each part of the layer (series of RC elements), as shown in Fig. 1(b) and (c), respectively. Thus, the transient responses of Eqs. (8) and (10) can be obtained by the use of Laplace transform methods, based on the assumption that the electrical circuits are linear and time invariant (LTI), as discussed in the next section. On the other hand, Eqs. (9) and (11) represent, respectively, a part of the total current and voltage for the surface and normal time-constant distributions electrically modeled in the equivalent circuits of Figs. 1(b) and 1(c), respectively. Continuing with the analysis, we next point out that the multi-exponential dynamics of Eqs. (9) and (11), without loss of generality, becomes negligibly small at the settling or steady-state time:

$$t_{ss} = -R_{Th}C_{limit}ln(\varepsilon) \tag{12}$$

resulting in a limiting RC-behavior (refer to Fig. 1(d)). ε represents the allowance tolerance that typically, in control engineering, takes values from ±5 % ($t_{ss} = 3R_{Th}C_{limit}$) to ±1 % ($t_{ss} = 5R_{Th}C_{limit}$) [1,44] and the limit capacitance, depending on the time-constant distribution, is [35,47]:

$$C_{limit} = \begin{cases} \sum_i C_i & \text{surface distribution} \\ \sum_i \frac{1}{C_i} & \text{normal distribution} \end{cases} \tag{13}$$

that theoretically denotes infinite series (electrical circuits of Fig. 1(b) with $R_s \to 0$ and Fig. 1(c) when $t \to 0$ or $\omega \to \infty$) but really have an end due to its physical meaning (refer to Fig. 1(d)). For the case of the resistivity properties, it follows that $R_s = \sum_i R_{s,i}$ and $R_p = \left[\sum_i \left({}^{1}/_{R_{s,i}+R_{p,i}}\right)\right]^{-1} - R_s$ (Fig. 1(b)) or $R_p = \sum_i R_{p,i}$ (Fig. 1(c)). Note that the Thévenin resistance in Eqs. (8)–(11) under voltage or current stimulation, respectively, correlates with surface or normal time-constant distribution (see above).

Now the question is: What is the adequate numerical approximation of the steady-state time considering CPE effects? As the CPE introduced in the modified Randles circuit of Fig. 1(a) involves a fractional-order derivative, the Mittag-Leffler function arises naturally to govern now the transient responses [48], replacing, respectively, the continuous distribution of elementary exponential relaxations $e^{-\frac{R_{s,i}+R_{p,i}}{R_{s,i}R_{p,i}C_i}t}$ and $e^{-\frac{t}{R_{p,i}C_i}}$ that predict microscale behavior by $E_\alpha\left[-\left({}^{(R_s+R_p)}/_{R_sR_pQ}t^\alpha\right)\right]$ and $E_\alpha\left[-{}^{t^\alpha}/_{R_pQ}\right]$ evidenced by macroscale observations [49,50]. Therefore, Eqs. (8)–(11) expressed in terms of a characteristic time constant τ_0, yield:

$$i(t) = \frac{\Delta V}{R_s+R_p}\left(1+\frac{R_p}{R_s}E_\alpha\left[-\left(\frac{t}{\tau_0}\right)^\alpha\right]\right) \tag{14}$$

$$i_{CPE}(t) = \frac{\Delta V}{R_s}E_\alpha\left[-\left(\frac{t}{\tau_0}\right)^\alpha\right] \tag{15}$$

$$v(t) = \Delta IR_s + \Delta IR_p\left(1-E_\alpha\left[-\left(\frac{t}{\tau_0}\right)^\alpha\right]\right) \tag{16}$$

$$v_{CPE}(t) = \Delta IR_p\left(1-E_\alpha\left[-\left(\frac{t}{\tau_0}\right)^\alpha\right]\right) \tag{17}$$

where

$$E_\alpha\left[-\left(\frac{t}{\tau_0}\right)^\alpha\right] = \sum_{k=0}^{\infty}\frac{\left[-\left(\frac{t}{\tau_0}\right)^\alpha\right]^k}{\Gamma(\alpha k+1)} \tag{18}$$

resulting in the MacLaurin series of the exponential function for $\alpha = 1$. Remember that the dispersion of capacitances, independently of the origin, can be mimicked by an infinite series of RC circuits (Figs. 1(b) and (c)) and thus, the behavior of the Mittag-Leffler function, corresponding to Cole-Cole relaxation pattern, resembles multi-exponential terms (Eqs. (8)–(11)). Another non-Debye phenomenological expressions usually used to fit the experimental impedance data with dissipative resistive-capacitive properties are the Davidson-Cole, Havriliak-Negami, Fox *H*-functions, Jurlewicz-Weron-Stanislawsky, and *q*-deformed models [51]. In effect, all these theoretical patterns with extra degrees of freedom to capture the electrical response of dynamical systems also lead to depressed arcs and dispersive time decay laws but now given in terms of more complex analytical responses as they typically model a combination of fractional-order processes. The Cole-Cole and Mittag-Leffler forms, related to the original version of the CPE under study here, can be indeed expressed in terms of all these advanced expressions with exact, closed form analytical representations. However, the special functions used here represent the most realistic and computationally efficient solutions to characterize these simple dispersive processes of capacitive origin. In electrical terms, the advanced mathematical functions previously indicated underlie non-conventional modified CPE versions [52] that would further generalize the concept of limit capacitance but are beyond the scope of this work.

Another important difference between the charging process of a capacitor and the corresponding CPE is the physical meaning of the time constants. In a RC circuit ($Q = C$ and $\alpha = 1$), the transient dynamics is characterized by a single time constant, $\tau_0 = R_{Th}C$ (δ-function). Nevertheless, as mentioned above, the time constant, when the CPE emerges, for example, in the modified Randles circuit of Fig. 1(a), shows a distribution in the τ-domain [53] with a maximum value of:

$$\tau_0 = (R_{Th}Q)^{1/\alpha} = \begin{cases} \left(\frac{R_sR_p}{R_s+R_p}Q\right)^{1/\alpha} & \text{3D dispersion (applied voltage)} \\ (R_pQ)^{1/\alpha} & \text{2D dispersion (current stimulation)} \end{cases} \tag{19}$$

visible, for example, through a plot of distribution of relaxation times (DRT) [54]; $\tau_i = {}^{R_{s,i}R_{p,i}C_i}/_{R_{p,i}+R_{s,i}}$ or $\tau_i = R_{p,i}C_i$ for the electrical circuits of Figs. 1(b) and 1(c), respectively. Indeed, the results of Eq. (6) are obtained by equating τ_0 under ideal ($\alpha = 1$) and dispersive conditions ($0 < \alpha < 1$), i.e., $R_{Th}C_{eff} = (R_{Th}Q)^{1/\alpha} \to C_{eff} = R_{Th}^{-1}(R_{Th}Q)^{1/\alpha}$ [35,55].

However, the Mittag-Leffler function is problematic for the transient analysis of electrical circuits due to its asymptotic inverse power-law behavior at long time scales [56]:

$$E_\alpha\left[-\left(\frac{t}{\tau_0}\right)^\alpha\right] \sim \sum_{k=1}^{\infty}(-1)^{k-1}\frac{\left[-\left(\frac{t}{\tau_0}\right)^\alpha\right]^{-k}}{\Gamma(1-\alpha k)}, \left({}^{t}/_{\tau_0}\right)\to\infty \tag{20}$$

in contrast to the classical exponential function, $e^{-\frac{t}{\tau_0}} \to 0$ for $\left({}^{t}/_{\tau_0}\right)\to\infty$. In fact, this special function of fractional calculus represents in our case the continuous charge process of infinitesimal capacitors but, although the characteristic steady-state time seems to diverge [31], the "number of capacitors" has to be finite from a physical point of view. To this end, a settling time with an asymptotic behavior estimated from the first term of the asymptotic series of Eq. (20),

$$E_\alpha\left[-\left(\frac{t}{\tau_0}\right)^\alpha\right] \sim \frac{\left({}^{t}/_{\tau_0}\right)^{-\alpha}}{\Gamma(1-\alpha)} \tag{21}$$

was introduced in [57]:

$$t_{ss} = \tau_0[\varepsilon\Gamma(1-\alpha)]^{-1/\alpha} \tag{22}$$

that depending of the origin in the variation of properties (along or normal to the surface of the material) or the nature of stimuli (current or voltage) can also give rise to different values in the time delay [58]. From our point view, both concepts are related in the formation of the CPE with the following characteristic values under steady-state conditions $i_{CPE}(t_{ss}) = 0$ A and $v_{CPE}(t_{ss}) = \Delta I R_p$ in Eqs. (15) and (17), respectively. Although not highlighted, the pseudo-equilibrium time derived above is valid only as long as $R_p \gg R_s$ for 3D capacitance dispersions; otherwise, the ratio R_p/R_s in Eq. (14) would be much lower or close to unity, resulting in inconsistent values of t_{ss} found by the approximation of Eq. (20). Furthermore, R_{Th} must be constituted by internal resistances of the system since external components (e.g., auxiliary resistances used in the charge/discharge of capacitive energy storage devices) would modify the value of the time constants associated to the relaxation processes and, therefore, the estimation of the limit capacitance of the CPE. A more general description of the asymptotic behavior of this type of relaxation fractional dynamics, in terms of the Mittag-Leffler function, can be found in [59]. Note also that the asymptotics of $E_\alpha\left[-\left(t/\tau_0\right)^\alpha\right]$ for $t \gg \tau_0$ modeled by Eq. (20) is only visible in experimental conditions if there are no additional phenomena at even longer time scales (e.g., slow diffusion processes [60] or additional R-CPE effects [58,61]) that would make diverging characteristics emerge in the transient responses due to the combination of two or more overlapping processes with different internal time scales. Analogously, this would occur with simple distorted capacitive semicircles modified by additional forms, such as double arcs, loops, spirals, hooks or curl-backs [62], for $\omega \ll 1/\tau_0$ in immittance measurements. However, this situation is beyond the scope of this work, which is based on the analysis of physical systems, electrically modeled by the simplified Randles circuit with CPE effects.

From a comparison of Eqs. (12) and (22) and using Eqs. (6) and (19), the limit capacitance associated with the CPE can therefore be expressed as:

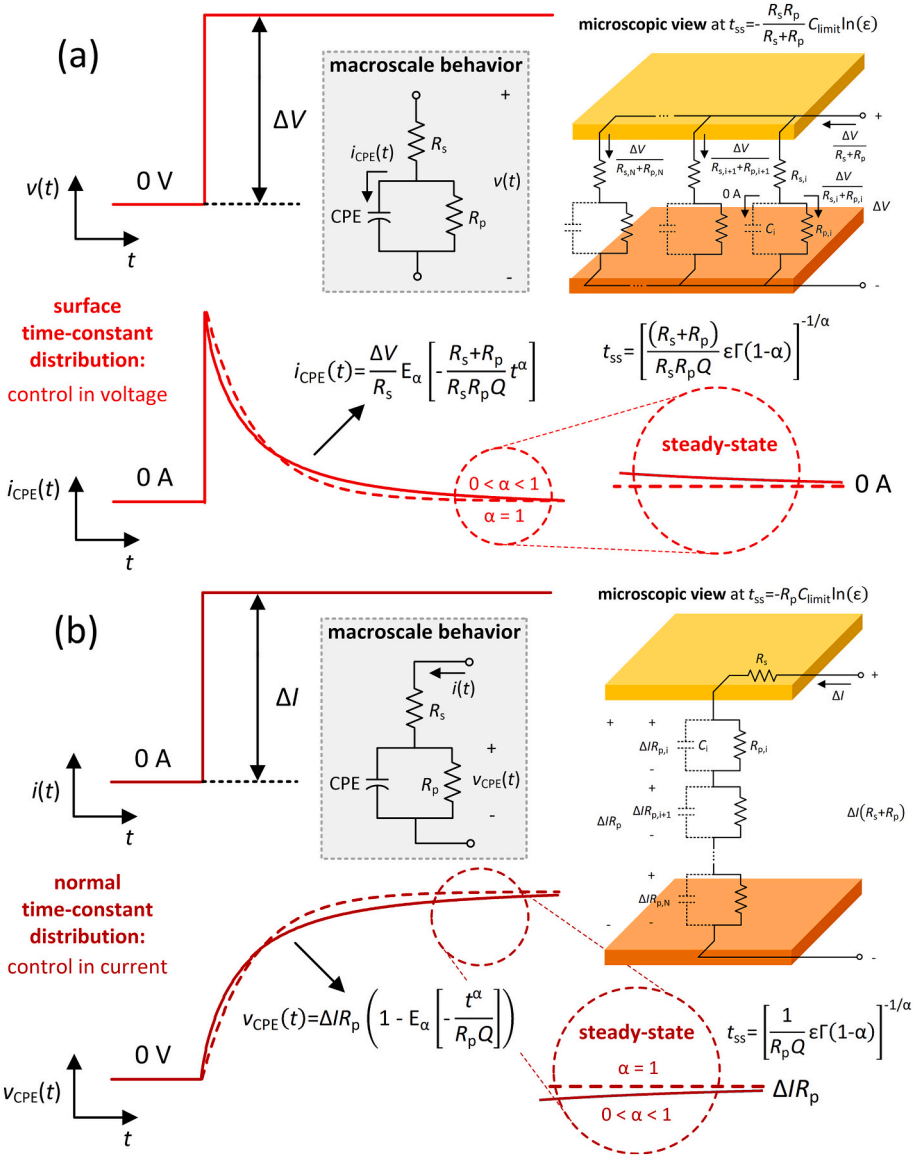

Fig. 2. Schematic representation of (a) surface and (b) normal time-constant distributions under voltage- and current-controlled excitations, respectively. Relaxation processes correspond to time-domain responses of the CPE ($i_{CPE}(t)$ and $v_{CPE}(t)$) at macroscopic level. Insets show the zoomed-in views of transient dynamics of the variables under study at long time scales when, by putting under a magnifying glass to CPE, all the capacitive elements contained in it are charged (steady-state conditions with the aid of Eqs. (19) and (23)).

$$C_{\text{limit}} = \left(-\frac{[\varepsilon\Gamma(1-\alpha)]^{-1/\alpha}}{ln(\varepsilon)} \right) C_{\text{eff}} \tag{23}$$

where, logically, the limit capacitance C_{limit} assumes a value $-[\varepsilon\Gamma(1-\alpha)]^{-1/\alpha}/ln(\varepsilon)$ higher than the effective capacitance C_{eff} estimated from the capacitance-CPE relations of Eq. (6). This view can be further elaborated, assuming the concept of "differential capacitance" ($\Delta C = C_{\text{limit}} - C$, where $C = Q$ for $\alpha = 1$) that emerges in the transition from ideal to dispersive capacitor in the delayed charge/discharge processes of fractional-order capacitive energy storage systems. We expect to develop this further improvement of the model in future works. Apart of this preliminary analysis, we should also point out that minute changes in the electrical elements or, specifically, alterations in the CPE exponent α are directly correlated to variations in material properties and non-idealities typically present in real-world scenarios (e.g., interface heterogenous kinetics in electrochemistry [45]), which would be easily detectable by Eq. (23) because it is very sensitive to changes in the value of the parameters. Inspired by the waveforms of current and voltage of the CPE derived from Eqs. (15) and (17), we show a circuit representation of a surface and normal time-constant distribution in Figs. 2(a) and (b), respectively, in which some capacitance elements are charged and thus not observed over an experimentally accessible time range until the value C_{limit} is reached at the time instant t_{ss} when, theoretically, capacitive effects are kinetically limited.

The ratio of $C_{\text{limit}}/C_{\text{eff}}$ is plotted *vs* α as a function of ε in Fig. 3. We observed that the relation limit-effective capacitance enlarged significantly with dropped CPE exponents (from ideal to Warburg-like behavior) and, in addition, showed a systematic increase as ε decreases for each α. Both trends are related to the width of the time-constant distribution quantified by the dispersive coefficient. For the case of an ideal capacitor, $C_{\text{limit}} \sim C_{\text{eff}}$. Of special interest is the sensitivity of the model in determining C_{limit} to the value of ε, shown in Fig. 3, in close relation to the error in the estimate of t_{ss} whose interpretation was confirmed by a variety of numerical simulations in [57]. It represents the most important limitation in our theoretical analysis, in addition to those inherent to the experimental techniques implemented (LTI conditions, stability, reproducibility or noise) that are explained later. As α decreases, the value of C_{limit} significantly increases as can be seen in Fig. 3, which could lead to over-estimations of the real value. In this case, it is therefore recommended to use high values of ε. The same situation occurs with α values close to the ideality, for which it is convenient to use "safer tolerance values". Note that one could gain greater accuracy by using higher order approximations of the general expansion of the Mittag-Leffler function at sufficiently long times in Eq. (20) –see Appendix A–, especially for values of α close to the ideal behavior (α→1) and low allowable tolerances; i.e., when our expression does not work ($C_{\text{limit}} < C_{\text{eff}}$ in Fig. 3) [57]. However, we prefer to use Eq. (23) because it captures, in a simple manner, the fundamental origin of the CPE in the vast majority of experimental observations through an analytical expression aligned with the famous theory of the effective capacitance, covering the concept of time-constant distribution. In any case, it is clear that the value of the limit capacitance C_{limit} scaled by C_{eff} tends to infinity as the value of the CPE exponent tends to zero.

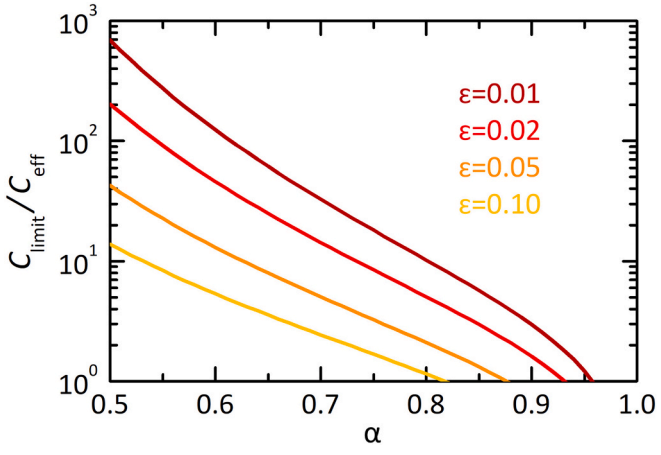

Fig. 3. Ratio of the limit capacitance to the associated effective value from Warburg-type behavior (α = 0.5) to ideal response (α = 1) for different values of the allowable tolerance ε.

Even though our method is clearly formulated, more theoretical work is indeed needed to analyze, for instance, the capacitive transient responses in a discrete form to obtain a consolidated interpretation of the limiting behavior of the CPE by independent mathematical perspectives. Fractional-order behavior involves the existence of inherent memory traces in the transient regime that increase when the fractional-order α decreases further away from 1 and fades out with time [37]. The transition from anomalous to ideal dynamics in the CPE occurs when the memory effects vanish and do not have any impact on the behavior of the system, converting it into a simply memoryless capacitor. Note that the theory proposed here can be used analogously to analyze CPE-type inductive phenomenology [63,64].

Finally, it is necessary to indicate that our model represents an alternative approach to capture the charge and energy characteristics under steady-state conditions of the CPE from the concept of limit capacitance. Several formulas have been proposed in the literature depending on the dominant factors that determine the value of these parameters, generally time-dependent [21,39,65,66]. From Eq. (22), it is possible to derive closed-form analytical solutions of the limit charge and energy of the dispersive capacitance, experimentally obtained by inspection as $q = \int_0^t i_{\text{exp}} dt$ and $W = \int_0^q v_{\text{exp}} dq$. Nevertheless, a much more systematic analysis is needed to make further progress in the elucidation of a definitive theory of the charge and energy of fractional-order electrical energy storage devices.

3. Results and discussion

Next, we apply Eq. (23) to representative examples of literature corresponding to surface and normal time-constant distributions for the determination of limit capacitance of the CPE via numerical simulations of impedance and transient responses. Specific cases pertaining to the field of electrochemistry and neurosciences were selected from previous works of the authors, where the parameter values were estimated by fitting experimental current/voltage transient responses (small-perturbation time-domain method) and the equivalent impedance spectra (frequency-resolved technique). For numerical simulations, we use MATLAB routines to evaluate the Mittag-Leffler function [67]. In any case, it is important to point out that there is an infinite number of materials and processes with intrinsic CPE effects in the literature for which the proposed model for estimating the limit capacitance can be applied since this widespread anomalous behavior is observable not only in electrochemistry and biological sciences but also in, for instance, electronics or physics. Before proceeding, a note on the number of limitations in the process of decoding experimental data with dispersive traces is in order. Due to the complex nature of real-world systems which also exhibit non-linear and time-variant features as explained in detail below, the electrical responses are not easy to model with unequivocal equivalent circuits with a clear physical origin. Different electrical models, based on multiple-RC circuits or time-dependent capacitances, can produce reconstructed impedances and time decays with CPE effects that are quite close to the original data [68,69]. This is an intrinsic problem of the methods themselves that affects the estimation of the limiting behavior of the dispersive capacitance under study. For this reason, a combination of different experimental techniques is

recommended to elucidate the operating mechanisms of dynamical systems, as developed here.

First, we study the case of a surface time-constant distribution through a typical electrode-electrolyte system for biomedical applications. Based on literature [49,50], we propose the following parameter values of the modified Randles circuit of Fig. 1a: $R_s = 10\,\Omega\,\mathrm{cm}^2$, $Q = 50\,\mu\mathrm{F}/(\mathrm{cm}^2\mathrm{s}^{1-\alpha})$, $\alpha = 0.85$, and $R_p = 200\,k\Omega\,\mathrm{cm}^2$, where, in this example, R_s and R_p represent the solution and charge-transfer resistances ($R_p = R_{ct}$), respectively, and CPE models the electrochemical double-layer capacitance ($C_{dl,i}$ at microscopic level). Fig. 4(a) exhibits the numerical simulations of the internal transient current, $i_{CPE}(t)$, through the CPE in response to an external potentiostatic step of $v(t) = 10$ mV. Note that the resulting current shown in Fig. 4(a) is experimentally inaccessible, being therefore estimated from the external current $i(t)$ and the impedance response (see below), measured in [49,50]. In any case, the obtained result adequately represents the expected behavior of the CPE. Use of Eq. (6) for surface distributions yields $C_{eff} = 13.08\,\mu\mathrm{F/cm}^2$ as an average value of the distribution of capacitance. From the CPE parameters and the resistances of the equivalent circuit, the limit capacitance of the electrochemical double layer under study was determined by application of Eq. (23) by using the 2 % criterion ($\varepsilon = 0.02$), resulting in $C_{limit} = 38.81\,\mu\mathrm{F/cm}^2$. For verification purposes, we have also determined the limit capacitance of the CPE from impedance measurements. Figs. 4(b) and 4(c) show the simulated electrical response in the frequency-domain represented using Cole-Cole admittance diagrams and Bode capacitance plots. In the Nyquist plot of Fig. 4(b), the capacitive semicircle is clearly depressed and, more importantly, the transition to a final value in the capacitive spectra shown in Fig. 4(c) suffers a significant deceleration due to self-scaling properties of the CPE response, reaching a pseudo-constant capacitance in the scale of several tens of $\mu\mathrm{F/cm}^2$ –values of capacitance between 10^{-5} and 10^{-4} F/cm^2 in Fig. 4(c)– [3,70] at sufficiently low frequencies. The interest parameters obtained using transient analysis are remarkably close to those found from frequency-resolved techniques.

For the case of a normal time-constant distribution through a surface layer, we select a neuronal membrane. The situation is illustrated in Fig. 5(a) via numerical computations in the voltage across the internal dispersive capacitance shown in Fig. 1(a) in response to a current step of $i(t) = 20$ nA. Simulated waveforms have been plotted using Eq. (16) with the following parameter values: $R_s = 1\,k\Omega\,\mathrm{cm}^2$, $Q = 1\,\mu\mathrm{F}/(\mathrm{cm}^2\mathrm{s}^{1-\alpha})$, $\alpha = 0.80$, and $R_p = 75\,k\Omega\,\mathrm{cm}^2$ [71]. Here, R_s is associated with the measurement process, CPE models the capacitance of the bilayer phospholipid structure ($C_{m,i}$ in a microscopic view), and R_p represents the membrane ionic permeability ($R_p = R_m$). The effective and limit capacitances found numerically to be 0.53 and 1.09 $\mu\mathrm{F/cm}^2$ (of the order found in literature [72,73]) which can be deducted from Eqs. (6) and (23) with an allowable tolerance band of ±5 % ($\varepsilon = 0.05$), respectively. For confirmation, we again show the frequency-domain responses in the plots of Figs. 5(b) (impedance) and 5(c) (capacitance-frequency results) which clearly indicate that the calculation of C_{limit} via transient analysis is similar to that predicted by impedance analysis as a reasonable low-frequency limit capacitance in this case. For this

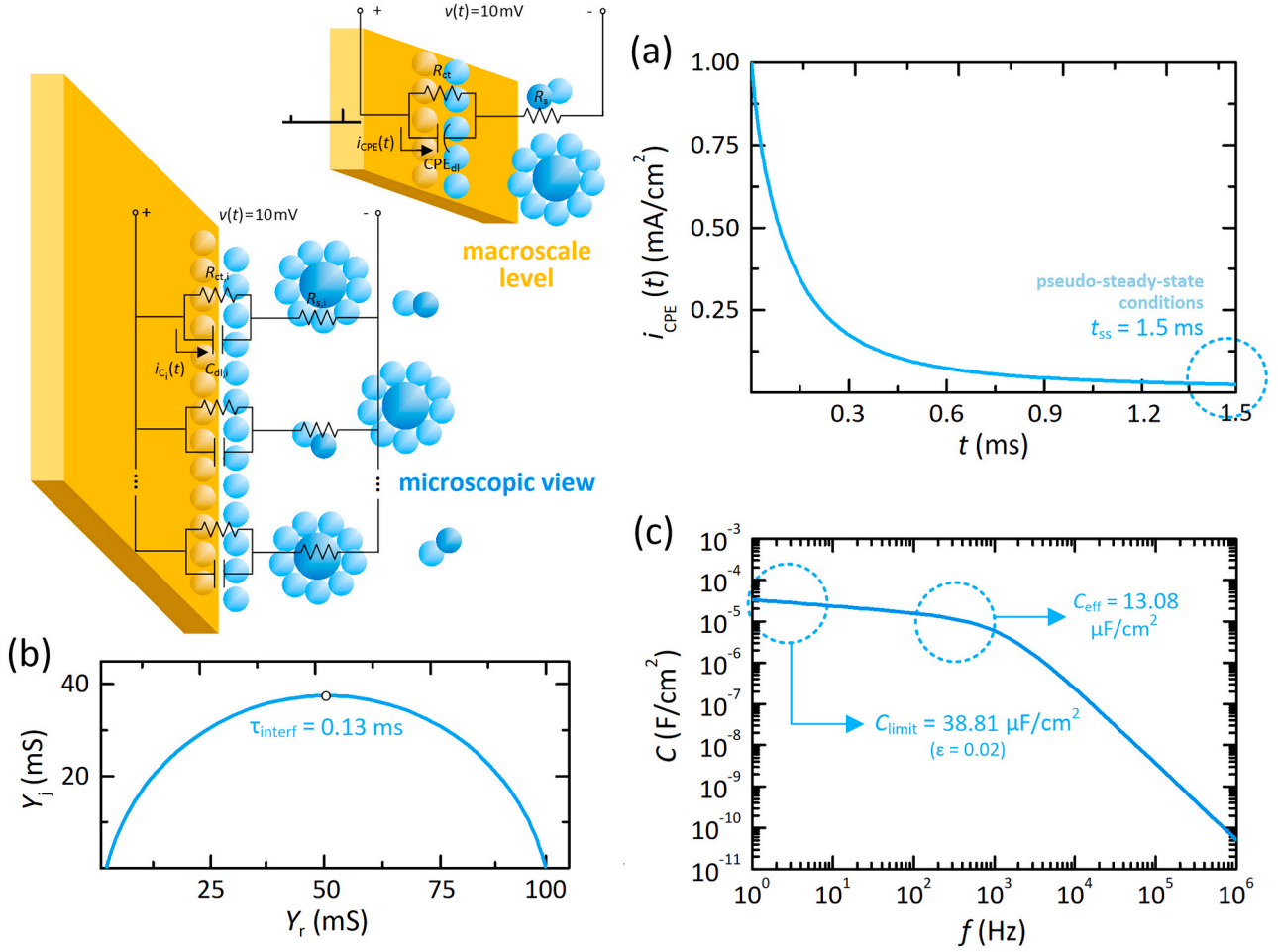

Fig. 4. Identification of limit capacitance for the electrochemical double-layer in a simple electrode-electrolyte interface. (a) Waveform of the CPE current in response to a step potential of 10 mV. (b) Nyquist plot and (c) capacitance Bode representation. In (a), the steady-state time is highlighted leading to the limit capacitance value indicated in (c). Also in (c) the effective capacitance is pointed, which was obtained from the relaxation time of (b).

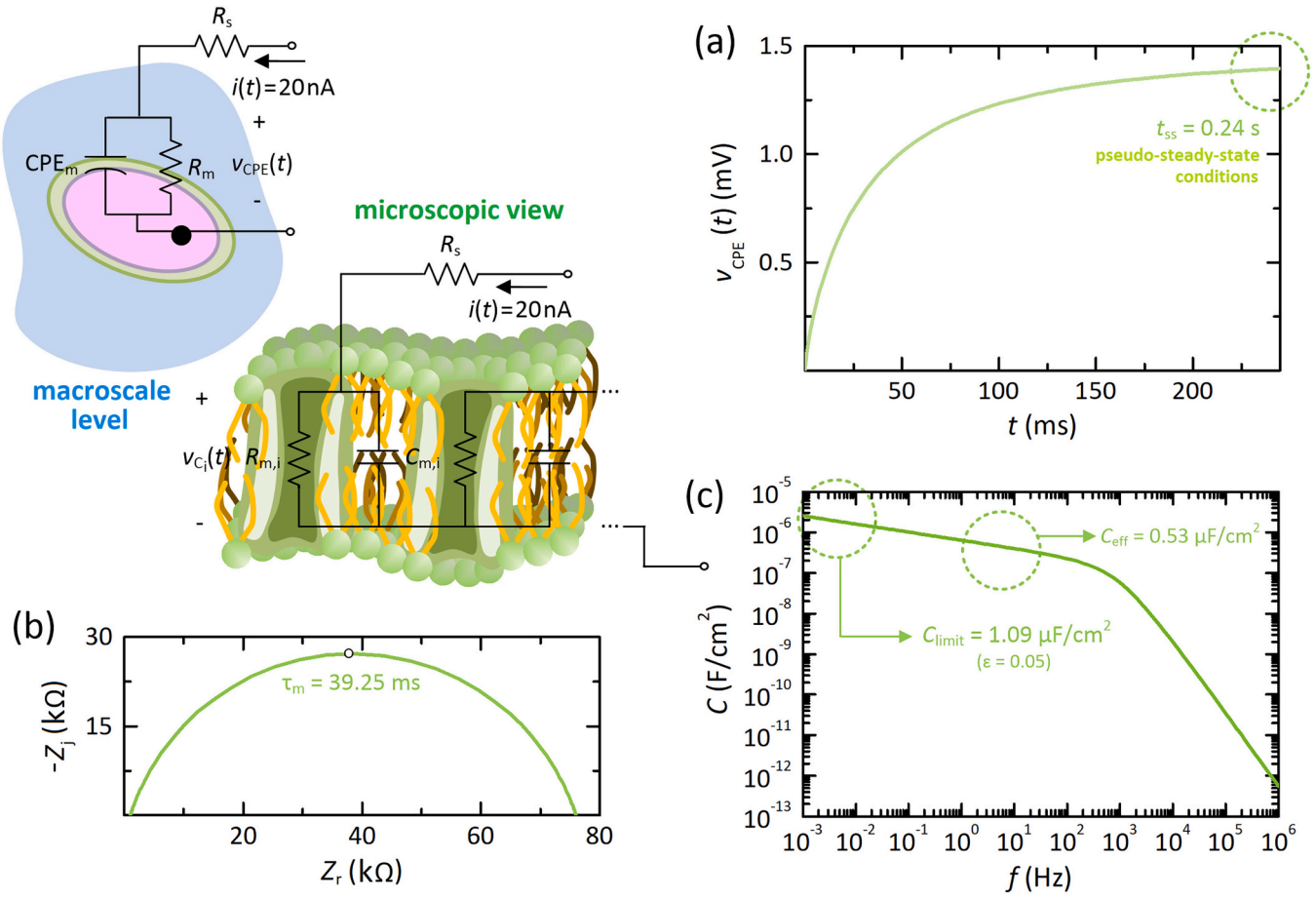

Fig. 5. Analysis of the CPE behavior of the cell membrane: (a) Transient-voltage response to a step current of 20 nA, (b) complex plane impedance plot, and (c) capacitance modeling in Bode representation, indicating, in all the cases, the characteristic parameters for the determination of the limit capacitance.

representative case, the transient response shown in Fig. 5(a) was obtained in [71] via patch-clamp recordings; however, the Nyquist and Bode plots shown in Fig. 5(b) and 5(c), respectively, have been reconstructed from the equivalent circuit obtained by using the time-domain technique. Regardless of this, we should point out that frequency-domain responses in the neuronal membrane simulated here exhibit the characteristic patterns of the CPE. As a final remark, it should be noted that small perturbation methods in time- and frequency-domain analyzed here are equivalent because the current-voltage expressions of all elements of the equivalent circuits are linear and independent of time and frequency [74].

The main advantage of the theory proposed here is that, as a final solution, it provides a very simple mathematical approach to obtain valuable information about the anomalous properties of real-world capacitive materials from a perspective physically coherent. This advantage is sometimes a weakness if a clear context for the treatment of experimental data is not available (see previous discussion about the selection of the value of ε). Unfortunately, capacitive effects in real-world applications are not analyzed properly in many published papers related to CPE. It is common to observe the inclusion of CPEs in equivalent circuits to fit complex plane impedance plots or transient responses with such as component selected *ad hoc* to obtain good agreements between experimental and simulated data without any contrasted base. The number of possible experimental scenarios is endless, and thus, there is a wide variety of readers working on the modeling of capacitive systems for which this technique may be useful. Here we developed a theoretical model, based on a series of criteria obtained from our experience, to indicate what should be the minimum guidelines when presenting correlations of a CPE behavior with ideal capacitive effects beyond the Q and α parameters and even the famous effective capacitance. When applying electrical measurements, one should try to provide a valid physical picture of the processes associated with, in this case, capacitive elements. Nevertheless, the basic theoretical framework describing the behavior of the CPE includes mathematical approaches that lead to infinite values, which is not appropriate from a physical perspective. Following the guidelines presented in this work should avoid undesirable situations where experimental data provide scarce knowledge and limited understanding of the phenomenology under study, including thus a real estimation of real-world capacitive processes with dispersive traces. In this way, we hope that this work provides a fundamental advance, from design to application, in scientific and technological areas in which capacitive behavior plays a key role.

As final remarks, we provide a discussion of the practical applicability of our model, starting from the general theory of LTI systems. In the electrical measurements of transient responses and impedance spectra under study here, the processes, although typically non-LTI, are, on the one hand, stabilized in an equilibrium state, obtaining thus linear responses by the small perturbation criterion. Therefore, nonlinearity and memory effects, characteristic of complex materials, do not come into play in the determination of the responses, allowing the consistent use of basic circuit theory to explain the underlying physical processes. The electrical responses depend only on the operating or bias point, leading to voltage-dependent electrical elements, as is the case here in the limit capacitance of the CPE. On the other hand, the time-invariant condition to adequately determine C_{limit} is logically fulfilled via data acquisition times sufficiently short in such a way that the systems can be considered "frozen" during the measurements. Typically, this specific

requirement is achieved by using Impedance Spectroscopy and even more so with time-domain measurements because the duration of the experiments is much shorter than that necessary to observe a change in the materials. Nevertheless, we should point out that the classical local-in-time effects of real-world systems may become a problem to reach extremely long times or significantly low frequencies in the limit capacitance scales for slow responding materials that are not entirely stable if their electrical properties change during the data acquisition time. This aspect is also intimately connected to the reproducibility of the electrical responses supporting the proposed model due to practical challenges (parasitic effects, noise, and other non-idealities) commonly encountered in experimental setups, particularly in the long-time relaxation patterns, and that could lead to a snapshot of the situation at a given moment. These effects would severely modify the capacitive properties that are crucial for system operation here. By following general good practices (e.g., use of a Faraday cage, adequately shielded connections and wires, high-quality potentiostats with an ultra-fast sampling resolution), materials can be however measured under controlled conditions to avoid a combination of variability pathways during the experiments.

4. Conclusions

Although different types of experimental techniques have long given us to understand the motion and interactions of electric charges in materials with an associated capacitive phenomenology, experimental data show that the internal dynamics is not as simple as we thought and that the micro-capacitances, equivalent to the "macro CPEs", exhibit values that are forever changing over a wide range. In the language of the energy-landscape model of materials, this observed dispersive dynamics leads to the famous "infinite capacitance paradox" of the CPEs that has not been fully elucidated yet. Here, we have developed a comprehensive exploration of the intricate nature of the CPE delineated in two fundamental archetypes (surface and normal time-constant distributions) rooted in distinctive transient responses. From our unifying framework that compares the charge processes of internal infinitesimal capacitors at the microscopic level (multi-exponential terms) with that of the macroscopic natural CPE (Mittag-Leffler function), we decipher the limit capacitance in real-world systems as disparate as electrochemical interfaces, biological media, or electronic devices, by using numerical approximations. In this sense, the capacitive characteristics of electrochemical double layers and cell membranes, as illustrative examples, have been determined here under simulated real-world operating conditions (CPE behavior), obtaining realistic values somewhat higher than conventional ones (20 and 1 $\mu F/cm^2$, respectively) found in classic textbooks that consider ideal conditions [70,75]. We hope that this work contributes to the broader understanding of the anomalous and dispersive capacitance (CPE) observed in very wide range of storage energy systems (also in, for instance, fuel cells, supercapacitors, or batteries), to be physically consistent on the basis of a limiting ideal behavior.

CRediT authorship contribution statement

Enrique H. Balaguera: Writing – review & editing, Writing – original draft, Visualization, Validation, Supervision, Software, Project administration, Methodology, Investigation, Funding acquisition, Formal analysis, Conceptualization. **Anis Allagui:** Writing – review & editing, Validation, Formal analysis.

Declaration of competing interest

The authors declare that they have no known competing financial interests or personal relationships that could have appeared to influence the work reported in this paper.

Data availability

Data will be made available on request.

Acknowledgements

This work has received funding from the Universidad Rey Juan Carlos, project number M2993.

Appendix A. Numerical refinement in the calculation of the limit capacitance

A refined value for the steady-state time t_{ss} can be found from the first two non-vanishing terms of Eq. (20),

$$\mathrm{E}_{\alpha}\left[-\left(\frac{t}{\tau_0}\right)^{\alpha}\right] \sim \frac{\left(t/\tau_0\right)^{-\alpha}}{\Gamma(1-\alpha)} - \frac{\left(t/\tau_0\right)^{-2\alpha}}{\Gamma(1-2\alpha)} \tag{A.1}$$

yielding [57]:

$$t_{ss} = \tau_0 \left[\frac{\Gamma(-2\alpha)}{\Gamma(-\alpha)} + \sqrt{\left[\frac{\Gamma(-2\alpha)}{\Gamma(-\alpha)}\right]^2 + 2\varepsilon\alpha\Gamma(-2\alpha)}\right]^{-1/\alpha} \tag{A.2}$$

Therefore, we can obtain again the limit capacitance of the CPE, similarly to previous methodology, as:

$$C_{\mathrm{limit}} = \left(-(ln(\varepsilon))^{-1}\left[\frac{\Gamma(-2\alpha)}{\Gamma(-\alpha)} + \sqrt{\left[\frac{\Gamma(-2\alpha)}{\Gamma(-\alpha)}\right]^2 + 2\varepsilon\alpha\Gamma(-2\alpha)}\right]^{-1/\alpha}\right) C_{\mathrm{eff}} \tag{A.3}$$

which provides superior results than those of Eq. (23) for different values of α in the "capacitive region", except for the Warburg-like behavior ($\alpha = 0.5$) due to Gamma function is not defined at $\Gamma(-1)$.

A further comparison of the mathematical approach is presented below to validate the accuracy of the proposed transient analysis for determining the limit capacitance of the CPE. Specifically, we propose, based on the complete monotonicity of $\mathrm{E}_{\alpha}\left[-\left(t/\tau_0\right)^{\alpha}\right]$, to study the inverse generalized Mittag-Leffler function, $\mathrm{L}_{\alpha}(\mathrm{E}_{\alpha}[x]) = x$ with $x \geq 0$, defined as [76]

$$-\mathrm{L}_{\alpha}(x) \approx \frac{1}{2\Gamma(1-\alpha)x} - \frac{q_1^*}{2} + \sqrt{\left(\frac{q_1^*}{2} - \frac{1}{2\Gamma(1-\alpha)x}\right)^2 - q_0^*\left(1-\frac{1}{x}\right)} \tag{A.4}$$

and obtained via highly accurate global Padé approximations, whose coefficients are:

$$q_0^* = \frac{\frac{\Gamma(1+\alpha)}{\Gamma(1-\alpha)} - \frac{\Gamma(1+\alpha)\Gamma(1-\alpha)}{\Gamma(1-2\alpha)}}{\Gamma(1+\alpha)\Gamma(1-\alpha)-1}, q_1^* = \frac{\Gamma(1+\alpha) - \frac{\Gamma(1-\alpha)}{\Gamma(1-2\alpha)}}{\Gamma(1+\alpha)\Gamma(1-\alpha)-1} \tag{A.5}$$

By the same numerical procedure, we can obtain a reformulation of the settling time t_{ss} and the limit capacitance C_{limit} of the form:

$$t_{ss} = \tau_0[-\mathrm{L}_{\alpha}(\varepsilon)]^{1/\alpha} \tag{A.6}$$

$$C_{limit} = -C_{eff}\frac{[-\mathrm{L}_{\alpha}(\varepsilon)]^{1/\alpha}}{ln(\varepsilon)} \tag{A.7}$$

Now, the value of the limit capacitance is controlled by a ratio of logarithms (classical and the fractional version) which also yields a better estimate than that of Eq. (23) but a worse approach than of Eq. (A.3) for situations in which α is substantial [57]. In any case, both numerical approximations presented in Appendix A are much more complex to suggest a universal use by experimentalists.

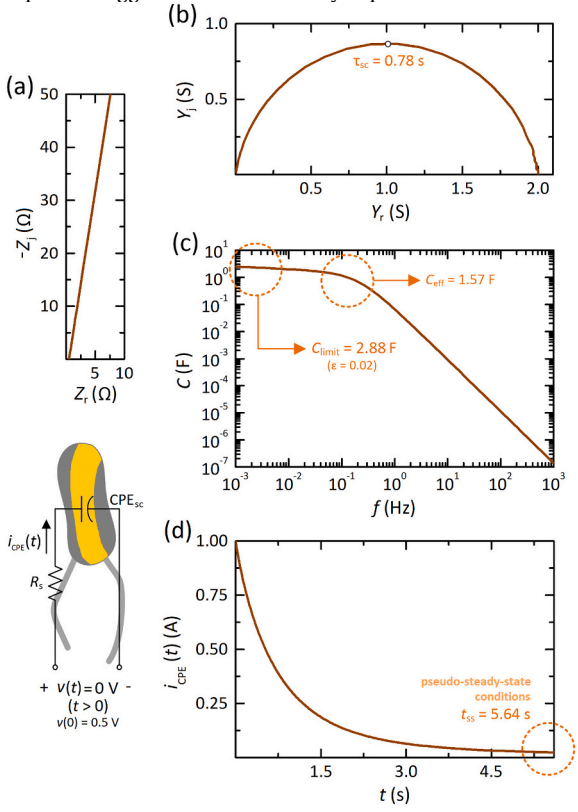

Fig. A.1. Numerical simulations of Nyquist plots in (a) impedance and (b) admittance representation of a supercapacitor. (c) Equivalent representation of the real part of the complex capacitance over a frequency range of interest. (d) Choroamperometric results during the discharge of the device for 0.5 V.

An example of energy storage devices that requires the use of numerical refinements in the estimation of the limit capacitance (α→1) are supercapacitors. The reason for using this last model is justified from the slightly inclined capacitive tail by a series R_s-CPE circuit (where $R_s = 0.5\ \Omega$, $Q = 1.6\ \mathrm{F/s^{1-\alpha}}$, $\alpha = 0.91$, and $R_p \to \infty$ in a 3 F, 2.7 V commercial supercapacitor [77]) and the equivalent depressed arc, typically obtained in the impedance and admittance representations [23], as shown in Figs. A.1(a) and A.1(b), respectively. Accordingly, the low-frequency plateau observed in Fig. A.1(c) can be related to the limit capacitance of the CPE found by using transient measurements. As an electric double-layer capacitor naturally exhibits a surface time-constant distribution, we therefore obtain the simulated transient current through the CPE, but now during a discharge phase with initial value of 0.5 V, as illustrated in Fig. A.1(d). The corresponding theoretical analysis is equivalent to a charge study; however, here we consider the discharge phase since it is the typical scenario in this technology [77,78]. If we consider that for $\varepsilon = 0.02$ the steady-state condition has been reached, then the settling time and the limit capacitance can be estimated from Eqs. (22) and (23), respectively, obtaining $t_{ss} = 5.64$ s and $C_{limit} = 2.88$ F with $C_{eff} = 1.57$ F, in agreement with the frequency resolved technique. For this case, we should clarify that the transient response and the complex plane plots shown in Fig. A.1 were obtained experimentally in [77], so our numerical simulations correspond to fits of such results (real behavior of the CPE).

References

[1] J.W. Nilsson, S.A. Riedel, Electric Circuits, Pearson, 2019.
[2] R. Metzler, J. Klafter, The random walk's guide to anomalous diffusion: a fractional dynamics approach, Phys. Rep. 339 (2000) 1–77.
[3] J. Wu, Understanding the electric double-layer structure, capacitance, and charging dynamics, Chem. Rev. 122 (2022) 10821–10859.
[4] A.L. Hodgkin, A.F. Huxley, A quantitative description of membrane current and its application to conduction and excitation in nerve, J. Physiol. 117 (1952) 500–544.
[5] H.P. Schwan, Electrical properties of tissue and cell suspensions, Adv. Biol. Med. Phys. 5 (1957) 147–209.
[6] S.M. Gateman, O. Gharbi, H. Gomes de Melo, K. Ngo, M. Turmine, V. Vivier, On the use of a constant phase element (CPE) in electrochemistry, Curr. Opin. Electrochem. 36 (2022) 101133.
[7] S. Wang, J. Zhang, O. Gharbi, V. Vivier, M. Gao, M.E. Orazem, Electrochemical impedance spectroscopy, Nat. Rev. Methods Primers 1 (2021) 1–21.
[8] F. Fabregat-Santiago, G. Garcia-Belmonte, I. Mora-Seró, J. Bisquert, Characterization of nanostructured hybrid and organic solar cells by impedance spectroscopy, Phys. Chem. Chem. Phys. 13 (2011) 9083–9118.
[9] A. Guerrero, J. Bisquert, G. Garcia-Belmonte, Impedance spectroscopy of metal halide perovskite solar cells from the perspective of equivalent circuits, Chem. Rev. 121 (2021) 14430–14484.
[10] S. Grimnes, O.G. Martinsen, Bioimpedance and Bioelectricity Basics, Academic Press, 2015.
[11] R.L. Magin, Fractional calculus models of complex dynamics in biological tissues, Comput. Math. Appl. 59 (2010) 1586–1593.
[12] E. Hernández-Balaguera, E. López-Dolado, J.L. Polo, Obtaining electrical equivalent circuits of biological tissues using the current interruption method, circuit theory and fractional calculus, RSC Adv. 6 (2016) 22312–22319.
[13] R. Metzler, Forever ageing, Nat. Phys. 12 (2016) 113–114.
[14] R. Metzler, J. Klafter, From stretched exponential to inverse power-law: fractional dynamics, Cole–Cole relaxation processes, and beyond, J. Non-Cryst. Solids 305 (2002) 81–87.
[15] K.S. Cole, Permeability and impermeability of cell membranes for ions, Cold Spring Harb. Symp. Quant. Biol. 8 (1940) 110–122.
[16] A.K. Jonscher, The 'universal' dielectric response, Nature 267 (1977) 673–679.
[17] S. Westerlund, L. Ekstam, Capacitor theory, IEEE T. Dielect. El. In. 1 (1994) 826–839.
[18] H. Rudolf, Applications of Fractional calculus in Physics, World Scientific, 2000.
[19] P. Córdoba-Torres, T.J. Mesquita, O. Devos, B. Tribollet, V. Roche, R.P. Nogueira, On the intrinsic coupling between constant-phase element parameters α and Q in electrochemical impedance spectroscopy, Electrochim. Acta 72 (2012) 172–178.
[20] A. Lasia, The origin of the constant phase element, J. Phys. Chem. Lett. 13 (2022) 580–589.
[21] M.E. Fouda, A. Allagui, A.S. Elwakil, S. Das, C. Psychalinos, A.G. Radwan, Nonlinear charge-voltage relationship in constant phase element, AEU Int. J. Electron. Commun. 117 (2020) 153104.
[22] M.D. Ortigueira, V. Martynyuk, V. Kosenkov, A.G. Batista, A new look at the capacitor theory, Fractal Fract. 7 (2023) 86.
[23] A. Allagui, T.J. Freeborn, A.S. Elwakil, M.E. Fouda, B.J. Maundy, A.G. Radwan, Z. Said, M.A. Abdelkareem, Review of fractional-order electrical characterization of supercapacitors, J. Power Sources 400 (2018) 457–467.
[24] S. Westerlund, Dead matter has memory!, Phys. Scr. 43 (1991) 174.
[25] E. Hernández-Balaguera, G. del Pozo, B. Arredondo, B. Romero, C. Pereyra, H. Xie, M. Lira-Cantú, Unraveling the key relationship between perovskite capacitive memory, long timescale cooperative relaxation phenomena, and anomalous J–V hysteresis, Sol. RRL 5 (4) (2021) 2000707.
[26] E. Hernández-Balaguera, B. Romero, M. Najafi, Y. Galagan, Analysis of light-enhanced capacitance dispersion in perovskite solar cells, Adv. Mater. Interfaces 9 (9) (2022) 2102275.
[27] J. Valsa, J. Vlach, RC models of a constant phase element, Int. J. Circ. Theor. App. 41 (2013) 59–67.
[28] S.H. Liu, Fractal model for the ac response of a rough interface, Phys. Rev. Lett. 55 (1985) 529–532.
[29] L. Nyikos, T. Pajkossy, Fractal dimension and fractional power frequency-dependent impedance of blocking electrodes, Electrochim. Acta 30 (1985) 1533–1540.
[30] P. Zoltowski, On the electrical capacitance of interfaces exhibiting constant phase element behaviour, J. Electroanal. Chem. 443 (1998) 149–154.
[31] A. Sadkowski, On the ideal polarisability of electrodes displaying cpe-type capacitance dispersion, J. Electroanal. Chem. 481 (2000) 222–226.
[32] G.J. Brug, A.L.G. van den Eeden, M. Sluyters-Rehbach, J.H. Sluyters, The analysis of electrode impedances complicated by the presence of a constant phase element, J. Electroanal. Chem. Interfacial Electrochem. 176 (1984) 275–295.
[33] C.H. Hsu, F. Mansfeld, Technical note: concerning the conversion of the constant phase element parameter Y0 into a capacitance, Corrosion 57 (2001) 747–748.
[34] J.-B. Jorcin, M.E. Orazem, N. Pébère, B. Tribollet, CPE analysis by local electrochemical impedance spectroscopy, Electrochim. Acta 51 (2006) 1473–1479.
[35] B. Hirschorn, M.E. Orazem, B. Tribollet, V. Vivier, I. Frateur, M. Musiani, Determination of effective capacitance and film thickness from constant-phase-element parameters, Electrochim. Acta 55 (2010) 6218–6227.
[36] A. Allagui, D. Zhang, A.S. Elwakil, Short-term memory in electric double-layer capacitors, Appl. Phys. Lett. 113 (2018) 253901.
[37] A. Allagui, D. Zhang, I. Khakpour, A.S. Elwakil, C. Wang, Quantification of memory in fractional-order capacitors, J. Phys. D. Appl. Phys. 53 (2019) 02LT03.
[38] A. Allagui, A.S. Elwakil, T.J. Freeborn, Supercapacitor reciprocity and response to linear current and voltage ramps, Electrochim. Acta 258 (2017) 1081–1085.
[39] A. Allagui, T.J. Freeborn, A.S. Elwakil, B.J. Maundy, Reevaluation of performance of electric double-layer capacitors from constant-current charge/discharge and cyclic voltammetry, Sci. Rep. 6 (2016) 38568.
[40] A. Sadkowski, Time domain responses of constant phase electrodes, Electrochim. Acta 38 (1993) 2051–2054.
[41] A. Lasia, Electrochemical Impedance Spectroscopy and its Applications, Springer, 2014.
[42] K. Biswas, S. Sen, P.K. Dutta, Realization of a constant phase element and its performance study in a differentiator circuit, IEEE Trans. Circuits Syst. II (53) (2006) 802–806.
[43] F.F. Kuo, Network Analysis and Synthesis, Wiley, 1962.
[44] K. Ogata, Modern Control Engineering, Prentice Hall, 2010.
[45] V. Vivier, M.E. Orazem, Impedance analysis of electrochemical systems, Chem. Rev. 122 (2022) 11131–11168.
[46] B. Hirschorn, M.E. Orazem, B. Tribollet, V. Vivier, I. Frateur, M. Musiani, Constant-phase-element behavior caused by resistivity distributions in films, ECS Trans. 28 (2010) 77.
[47] H. Liao, W. Watson, A. Dizon, B. Tribollet, V. Vivier, M.E. Orazem, Physical properties obtained from measurement model analysis of impedance measurements, Electrochim. Acta 354 (2020) 136747.
[48] R. Gorenflo, A.A. Kilbas, F. Mainardi, S.V. Rogosin, Mittag-Leffler Functions, Related Topics and Applications, Springer-Verlag, 2014.
[49] E. Hernández-Balaguera, J.L. Polo, On the potential-step hold time when the transient-current response exhibits a Mittag-Leffler decay, J. Electroanal. Chem. 856 (2020) 113631.
[50] E. Hernández-Balaguera, J.L. Polo, A generalized procedure for the coulostatic method using a constant phase element, Electrochim. Acta 233 (2017) 167–172.
[51] R. Garrappa, F. Mainardi, M. Guido, Models of dielectric relaxation based on completely monotone functions, Fract. Calc. Appl. Anal. 19 (2016) 1105–1160.
[52] A. Allagui, A.S. Elwakil, C. Psychalinos, Decoupling the magnitude and phase in a constant phase element, J. Electroanal. Chem. 888 (2021) 115153.
[53] M.L. Sartorelli, A.M. Cutrim Gomes, M. de Pauli, C.P. da Silva Reis, R.B. Serpa, F. Toledo Reis, E.F. Jasinski, L.N. Chavero, R.L. Cavalcante, D. Galvão, Z. Ocubo Raulino, Y. Zhou, Y. Feng, T. von Windheim, M. Vasquez Sanchez, E. Ngaboyamahina, J.J. Amsden, C.B. Parker, J.T. Glass, Model-free capacitance analysis of electrodes with a 2D+1D dispersion of time constants, Electrochim. Acta 390 (2021) 138796.
[54] B.A. Boukamp, Distribution (function) of relaxation times, successor to complex nonlinear least squares analysis of electrochemical impedance spectroscopy? J. Phys. Energy. 2 (2020) 042001.
[55] M.N. Kakaei, J. Neshati, A.R. Rezaierod, On the extraction of the effective capacitance from constant phase element parameters, Prot. Met. Phys. Chem. Surf. 54 (2018) 548–556.
[56] A. Erdélyi, Higher Transcendental Functions, McGraw-Hill, 1955.
[57] E. Hernández-Balaguera, Numerical approximations on the transient analysis of bioelectric phenomena at long time scales via the Mittag-Leffler function, Chaos, Solitons Fractals 145 (2021) 110768.
[58] E. Hernández-Balaguera, L. Muñoz-Díaz, C. Pereyra, M. Lira-Cantú, M. Najafi, Y. Galagan, Universal control strategy for anomalous ionic-electronic phenomenology in perovskite solar cells efficiency measurements, Mater. Today Energy 27 (2022) 101031.
[59] F. Mainardi, Fractional relaxation-oscillation and fractional diffusion-wave phenomena, Chaos, Solitons Fractals 7 (1996) 1461–1477.
[60] A.A. Moya, Identification of characteristic time constants in the initial dynamic response of electric double layer capacitors from high-frequency electrochemical impedance, J. Power Sources 397 (2018) 124–133.
[61] E. Hernández-Balaguera, B. Romero, B. Arredondo, G. del Pozo, M. Najafi, Y. Galagan, The dominant role of memory-based capacitive hysteretic currents in operation of photovoltaic perovskites, Nano Energy 78 (2020) 105398.
[62] E. Hernández-Balaguera, J. Bisquert, Time transients with inductive loop traces in metal halide perovskites, Adv. Funct. Mater. 34 (6) (2024) 2308678.
[63] E. Hernández-Balaguera, Fractional model of the chemical inductor, Chaos, Solitons Fractals 172 (2023) 113470.
[64] E. Hernández-Balaguera, B. Arredondo, C. Pereyra, M. Lira-Cantú, Parameterization of the apparent chemical inductance of metal halide perovskite solar cells exhibiting constant-phase-element behavior, J. Power Sources 560 (2023) 232614.
[65] M.E. Fouda, A.S. Elwakil, A.G. Radwan, A. Allagui, Power and energy analysis of fractional-order electrical energy storage devices, Energy 111 (2016) 785–792.
[66] E.B. Marthins, S. Holm, Difference between charge-voltage relations of ordinary and fractional capacitors, Fractal Fract. 7 (11) (2023) 781.
[67] I. Podlubny, I. Petrás, T. Skovránek, Fitting of experimental data using Mittag-Leffler function, in: Proceedings of the 13th International Carpathian Control Conference, 2012, pp. 578–581.

[68] S. Holm, T. Holm, O.G. Martinsen, Simple circuit equivalents for the constant phase element, PLoS One 16 (3) (2021) e0248786.
[69] J.A. López-Villanueva, P. Rodríguez-Iturriaga, L. Parrilla, S. Rodríguez-Bolívar, A compact model of the ZARC for circuit simulators in the frequency and time domains, AEU Int. J. Electron. Commun. 153 (2022) 154293.
[70] E. Barsoukov, J.R. Macdonald, Impedance Spectroscopy: Theory, Experiment, and Applications, John Wiley & Sons, 2005.
[71] E. Hernández-Balaguera, H. Vara, J.L. Polo, Identification of capacitance distribution in neuronal membranes from a fractional-order electrical circuit and whole-cell patch-clamped cells, J. Electrochem. Soc. 165 (12) (2018) G3104–G3111.
[72] L.J. Gentet, G.J. Stuart, J.D. Clements, Direct measurement of specific membrane capacitance in neurons, Biophys. J. 79 (2000) 314–320.
[73] R.L. Magin, Fractional calculus in bioengineering, part 2, Crit. Rev. Biomed. Eng. 32 (2004) 105–193.
[74] A. Allagui, A.S. Elwakil, H. Eleuch, Highlighting a common confusion in the computation of capacitance of electrochemical energy storage devices, J. Phys. Chem. C 125 (2021) 9591–9592.
[75] E.R. Kandel, J.H. Schwartz, T.M. Jessell, S.A. Siegelbaum, A.J. Hudspeth, Principles of Neural Science, McGraw-Hill (Health Professions Division), 2012.
[76] C. Zeng, Y.Q. Chen, Global Padé approximations of the generalized Mittag-Leffler function and its inverse, Fract. Calc. Appl. Anal. 18 (2015) 1492–1506.
[77] M.E. Fouda, A. Allagui, A.S. Elwakil, A. Eltawil, F. Kurdahi, Supercapacitor discharge under constant resistance, constant current and constant power loads, J. Power Sources 435 (2019) 226829.
[78] A.A. Moya, Nonlinear charge-voltage relationships in electric double layer capacitors performing under constant load resistance, J. Energy Storage 71 (2023) 108136.